Nanoparticles impact on miscible viscous fingering with absorbing boundary condition at inlet

Anoop Kumar [1,2] and Manoranjan Mishra [1,*]
[1]Department of Mathematics, Indian Institute of Technology Ropar, Rupnagar-140001, Punjab, India
[2]Department of Mathematics, Government College Barwala (Panchkula), 134118, Haryana, India

(Received 30 July 2021; accepted 17 March 2022; published 4 April 2022)

The addition of nanoparticles in fluids significantly influences the fluid's viscosity and can be helpful to control viscosity-driven instability. In this work, we analyze how such nanoparticles modulate viscosity and impact miscible viscous fingering (VF) dynamics. We consider the flow configuration such that the Hele-Shaw cell is initially filled with a viscous fluid and then displaces it with other viscous fluid-carrying nanoparticles through the inlet boundary, which corresponds to the absorbing boundary condition. A closed-form solution of base-state flow using the Laplace-transform method is obtained, which overcomes the discrepancy of the base-state solution known in the form of an infinite series as available in the literature. Due to the time-dependency and nonmonotonic nature of the base state, nonmodal linear stability analysis in the self-similar domain is used to determine the onset time of instability. In this work, the effects of various governing flow parameters such as nanoparticles diffusive coefficient (α_{np}), effective log-mobility ratio (R), and deposition rate of nanoparticles (Da_{dep}) on the instability are studied. Our finding suggests that the onset occurs early with increasing Da_{dep} for $\alpha_{\text{np}} > 1$, whereas such onset time is a nonmonotonic function of Da_{dep} for smaller values of α_{np}. In addition, our results indicate that the onset time is a nonmonotonic function of α_{np} for the smaller value of Da_{dep}, whereas such onset time is an increasing function of α_{np} for the larger value of Da_{dep}. Further, nonlinear simulations are performed using COMSOL MULTIPHYSICS, and the nonmonotonic nature on the onset of instability for different α_{np} is observed which is in good agreement with the linear stability analysis results. The present investigation removes various inconsistencies in the literature about the impact of the nanoparticles on VF with the quasi-steady-state approximation.

DOI: 10.1103/PhysRevFluids.7.044001

I. INTRODUCTION

In porous media, instability is often observed at the fluid-fluid interface when a less viscous fluid displaces a more viscous fluid, known as viscous fingering (VF) instability [1,2]. Conversely, when a more viscous fluid displaces a less viscous fluid, the fluid-fluid interface remains stable. In this work, we assume fluids are miscible and incompressible. In addition, fluid-fluid displacement is considered rectilinear. VF is significantly observable in various displacement processes such as in enhanced oil recovery [2], chromatography separation techniques [3], CO_2 sequestration in the underground reservoir [4,5], and contaminant transport in aquifers [6], to name a few. A Hele-Shaw cell is commonly used in the laboratory to study such interfacial phenomena in the miscible displacement process. In most experiments, the Hele-Shaw cell is first filled with one fluid and displaces it with another fluid through the inlet boundary. So in this work, we considered the flow configuration taken by Ghesmat *et al.* [7] where initially a more viscous fluid filled in the

*manoranjan@iitrpr.ac.in

domain and displaces it with other less viscous fluid-carrying nanoparticles. However, Dastvareh and Azaiez [8] and Sabet *et al.* [9] studied the impact of nanoparticles by considered another type of flow configuration where one more viscous semi-infinite fluid displaced by other less viscous semi-infinite fluid-carrying nanoparticles. There is a difference in the boundary condition at the inlet, where the absorbing boundary condition is used by Ghesmat *et al.* [7], and the reflective boundary is used by Dastvereh and Azaiez [8] and Sabet *et al.* [9].

Nanofluid flows in porous media have vast literature in thermal convection, medical science, and various others [10]. But recently, nanofluid flows in the displacement process have attracted the interest of many authors, which can be helpful in enhanced oil recovery [11], chromatography separation techniques, CO_2 sequestration, and many others [9]. Many researchers proposed the various mathematical modeling of such nanofluid flows. Kim *et al.* [12] advanced the study of the stability of nanofluids in Rayleigh-Benard convection by considering Soret and Dufour effects. Later, Ghesmat *et al.* [7] proposed a new model by considering the first-order removal term of nanoparticles due to interaction forces between particles [13]. According to Buongiorno [14], only the Brownian diffusion and the thermophoresis are the essential mechanisms in nanofluids. So, Dastvareh and Azaiez [15] also proposed a new model to discuss the thermophoretic effects of nanoparticles on nonisothermal flows using nonlinear simulations in the absence and presence of deposition of particles. Further, Zargartaleb and Azaiez [16] investigate nanoparticle flow behavior at the mesoscopic scale using a probabilistic model by considering the nanoparticle's size and surface energy along with the local temperature of the system. The role of reactive nanoparticles on the miscible front is explored in the literature recently [17–20]. Further, Jangir *et al.* [21] studied the miscible displacement by nanofluid with concentration-dependent diffusivity. Literature of the nonlinear simulations of miscible VF widely exists [22–25]. To investigate the effects of nanoparticles on the dynamics of VF, Dastvareh and Azaiez [8] and Sabet *et al.* [9] perform their nonlinear simulations with reflective boundary condition at the inlet using the pseudospectral method; however, nonlinear simulations with the absorbing boundary condition at the inlet is not available in the literature yet.

Governing equations with absorbing boundary condition at the inlet described by Ghesmat *et al*. [7] is considered in this paper. Dastvareh and Azaiez [8] and Sabet *et al*. [9] also adopt the same set of governing equations with reflective boundary condition at the inlet to study the influence of nanoparticles on miscible VF. All the available literature on the linear stability analysis (LSA) of nanoparticles impact on miscible VF are performed under the quasi-steady-state approximation (QSSA) [7–9]. Further, study with the absorbing boundary case [7] is limited, and reported that their justification on instability is inapplicable [9]. To the best of our knowledge, there is a lack of comprehensive study of nonreactive nanoparticle influences on miscible VF due to the nonmonotonic nature and time dependence of base-state flow. Here, we assumed the parameters such that the double-diffusive effect between the displacing and displaced fluids can be ignored. Hence, we study the present problem mainly with the effects of three nondimensional parameters, nanoparticles diffusive coefficient (α_{np}), effective log-mobility ratio (R), and deposition rate of nanoparticles (Da_{dep}), on the miscible VF phenomena. Nanoparticles deposition (Da_{dep}) in porous media can be avoided using surfactants or surface charge technology, and nanoparticles deposition occurs when these techniques are not used [26]. So in this paper, we considered both cases, (i) $Da_{\mathrm{dep}} = 0$ and (ii) $Da_{\mathrm{dep}} \neq 0$.

In this paper, the impact of nanoparticles on the onset of miscible VF with the absorbing boundary conditions at the inlet is discussed. In Sec. II, the problem formulation is described by adopting the similar mathematical modeling of Ghesmat *et al.* [7]. Then in Sec. III, a closed form of the base-state solution is determined using the Laplace-transform method and compared with the base-state series solution utilizing the separation of variables method [7,27]. Due to the nonmonotonic time-dependent base state, the initial value problem (IVP) in the self-similar domain is solved to discuss the nanoparticles' effect on miscible VF in Sec. IV. Furthermore in Sec. V, the results of the nanoparticles diffusive coefficient (α_{np}), effective log-mobility ratio (R), and the deposition rate of nanoparticles (Da_{dep}) on the onset time are studied using IVP in the self-similar

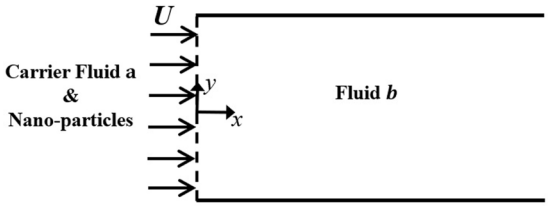

FIG. 1. Schematic diagram of two-dimensional flow configuration in homogeneous porous media, where the dashed line stands for the unperturbed nanofluid-fluid interface at initial time.

domain. In Sec. VI, nonlinear simulations are performed using the COMSOL MULTIPHYSICS software. General conclusions about the effect of nanoparticles on instability using nonmodal analysis are represented in Sec. VII.

In previous studies, it is reported that there exists a turning point of $\alpha_{\rm np} \approx 1$ such that nanoparticles diffusion ($\alpha_{\rm np}$) has a stabilizing and destabilizing effect before and after that turning value, respectively [7,9]. In contrast, Dastvareh and Azaiez [8,28] reported that $\alpha_{\rm np}$ has only a destabilizing impact on instability. Our finding of the α_{np} effect on instability is in line with the previous studies [7,9] for $Da_{\rm dep} < O(10^{-1})$. In addition, our studies suggest $\alpha_{\rm np}$ has only a stabilizing influence for $Da_{\rm dep} \gtrsim O(1)$. Previous studies [7–9] using the modal analysis reported that R and $Da_{\rm dep}$ has the stabilizing and the destabilizing effect on instability, respectively. In this paper, we also describe the more accurate results with justification regarding the effects of R and $Da_{\rm dep}$ on miscible VF.

II. MATHEMATICAL MODELING

A Hele-Shaw cell consists of two transparent parallel plates separated by a very small gap. A uniform rectilinear flow in a three-dimensional Hele-Shaw cell is mathematically analogous to two-dimensional flow in porous media [2,29]. Thus, the displacement of a viscous fluid by another viscous fluid laden with nanoparticles in the Hele-Shaw cell is studied by considering the flow in rectilinear homogeneous two-dimensional porous media [9,15]. The schematic of flow configuration is shown in Fig. 1, where initially the domain is filled with a fluid "b" of viscosity μ_b with molar concentration c_b and then displaced by injecting another fluid "a" of viscosity μ_a with molar concentration c_a carrying nanoparticles of viscosity $\mu_{\rm np}$ having molar concentration $c_{\rm np}$ with a longitudinal velocity U through the inlet boundary. In this study, fluids are considered miscible, Newtonian, nonreactive, neutrally buoyant, and incompressible. In addition, the permeability (κ) of the porous media and the diffusivity of the species are assumed constant.

The flow is described by the coupling of two physics interfaces, hydrodynamics and transport of solute species. The hydrodynamic part for incompressible flow and under the transient laminar flow condition is characterized by divergence-free velocity field for conservation of mass and Darcy's law to conserve the momentum in porous media. In addition, mass transport of the species c_a and c_b are governed by a convection-diffusion equation having diffusion coefficient D_a and D_b, respectively. Mass transport of the nanoparticles over a surface in the presence of interaction forces between particles is described by the convection-diffusion equation with an external force field [13,30]. In the present study, the governing equation for the nanoparticles of submicrometer size, a kinetic formulation for the interaction of nanoparticles, is used by considering the first-order removal term with diffusion coefficient $D_{\rm np}$ [7,31]. Thus, the governing equations of the problem are given as follows [7–9]:

$$\nabla \cdot \vec{u} = 0, \tag{1}$$

$$\nabla p = -\frac{\mu(c_a, c_b, c_{\rm np})}{\kappa}\vec{u}, \tag{2}$$

$$\frac{\partial c_a}{\partial t} + (\vec{u} \cdot \nabla)c_a = D_a \nabla^2 c_a, \tag{3}$$

$$\frac{\partial c_b}{\partial t} + (\vec{u} \cdot \nabla) c_b = D_b \nabla^2 c_b, \tag{4}$$

$$\frac{\partial c_{\rm np}}{\partial t} + (\vec{u} \cdot \nabla) c_{\rm np} = D_{\rm np} \nabla^2 c_{\rm np} - k_{\rm dep} c_{\rm np}, \tag{5}$$

where $\vec{u} = (u, v)$ is the two-dimensional velocity vector, p is the hydrodynamics pressure, μ is the dynamics viscosity of the solution, and $k_{\rm dep}$ is the nanoparticle deposition rate having unit $\rm s^{-1}$.

Initially the domain is filled with the fluid b, so the initial conditions are specified as

$$\vec{u}(x, y, t = 0) = (U, 0), \tag{6}$$

$$(c_a, c_b, c_{\rm np})(x, y, t = 0) = (0, c_{b0}, 0). \tag{7}$$

Moreover, the boundary conditions of the given problem are described as follows:

$$\vec{u}(x = 0, y, t) = (U, 0), \tag{8}$$

$$\vec{u}(x, y, t) = (U, 0) \quad \text{as} \quad x \to \infty, \tag{9}$$

$$(c_a, c_b, c_{\rm np})(x = 0, y, t) = (c_{a0}, 0, c_{\rm np0}), \tag{10}$$

$$\frac{\partial (c_a, c_b, c_{\rm np})}{\partial x} \to (0, 0, 0) \quad \text{as} \quad x \to \infty, \tag{11}$$

$$\frac{\partial (c_a, c_b, c_{\rm np})}{\partial y} \to (0, 0, 0), \ \frac{\partial v}{\partial y} \to 0 \quad \text{as} \quad y \to \pm\infty, \tag{12}$$

where c_{a0}, c_{b0}, and $c_{\rm np0}$ are the concentration of fluid a, fluid b, and nanoparticles at initial time $t = 0$. Here, Dirichlet boundary conditions at the inlet are specified, which is known as the absorbing boundary condition.

To complete the model, an Arrhenius-type relation is adopted between viscosity and solute species concentration c_a, c_b, $c_{\rm np}$ [7–9] as follows:

$$\mu(c_a, c_b, c_{\rm np}) = \mu_{\rm ref} e^{(R_a c_a + R_b c_b + R_{\rm np} c_{\rm np})/c_{a0}}, \tag{13}$$

where R_a, R_b, and $R_{\rm np}$ are log-mobility ratios defined as

$$R_a = \ln\left(\frac{\mu_{a0}}{\mu_{\rm ref}}\right), \qquad R_b = \left(\frac{c_{a0}}{c_{b0}}\right) \ln\left(\frac{\mu_{b0}}{\mu_{\rm ref}}\right), \qquad R_{\rm np} = \left(\frac{c_{a0}}{c_{\rm np0}}\right) \ln\left(\frac{\mu_{\rm np0}}{\mu_{\rm ref}}\right) \tag{14}$$

such as $\mu_{a0} = \mu(c_{a0}, 0, 0)$, $\mu_{b0} = \mu(0, c_{b0}, 0)$, $\mu_{\rm np0} = \mu(0, 0, c_{\rm np0})$. On the one hand, when $R_{\rm np} = 0$, $R_b > R_a$ represents the nanoparticles free system where a less viscous fluid displaces a more viscous fluid. On the other hand, $R_{\rm np} = 0$ with $R_b < R_a$ represents the nanoparticles free system where a more viscous fluid displaces a less viscous fluid. There is a total of 12 dimensional variables in the given problem (u, v, μ, c_a, c_b, $c_{\rm np}$, κ, p, D_a, D_b, $D_{\rm np}$, $Da_{\rm dep}$).

We nondimensionlized the governing equation using the diffusive characteristics scaling as the characteristics velocity U, characteristics length $\frac{D_a}{U}$, and characteristics time $\frac{D_a}{U^2}$. Also, viscosity, concentration, and pressure are nondimensionlized using $\mu_{\rm ref}$, c_{a0}, and $\frac{\mu_{\rm ref} D_a}{\kappa}$, respectively. Thus, the resulting dimensionless governing equation in the Eulerian frame are given as follows:

$$\nabla \cdot \vec{u} = 0, \tag{15}$$

$$\nabla p = -\mu \vec{u}, \tag{16}$$

$$\frac{\partial c_a}{\partial t} + (\vec{u} \cdot \nabla) c_a = \nabla^2 c_a, \tag{17}$$

$$\frac{\partial c_b}{\partial t} + (\vec{u}\cdot\nabla)c_b = \alpha_b \nabla^2 c_b, \tag{18}$$

$$\frac{\partial c_{\rm np}}{\partial t} + (\vec{u}\cdot\nabla)c_{\rm np} = \alpha_{\rm np}\nabla^2 c_{\rm np} - Da_{\rm dep} c_{\rm np}, \tag{19}$$

$$\mu = e^{R_a c_a + R_b c_b + R_{\rm np} c_{\rm np}}, \tag{20}$$

where the dimensionless parameters $\alpha_b = \frac{D_b}{D_a}$ and $\alpha_{\rm np} = \frac{D_{\rm np}}{D_a}$ represent the diffusive rate of fluid b and nanoparticles with respect to the diffusive rate of fluid a, respectively. Further, $Da_{\rm dep} = \frac{k_{\rm dep} D_a}{U^2}$ is the dimensionless deposition rate of nanoparticles. Also,

$$R_a = \ln\left(\frac{\mu_{a0}}{\mu_{\rm ref}}\right), \quad R_b = \frac{1}{\phi_b}\ln\left(\frac{\mu_{b0}}{\mu_{\rm ref}}\right), \quad R_{\rm np} = \frac{1}{\phi_{\rm np}}\ln\left(\frac{\mu_{\rm np0}}{\mu_{\rm ref}}\right), \quad \phi_b = \frac{c_{b0}}{c_{a0}}, \quad \phi_{\rm np} = \frac{c_{\rm np0}}{c_{a0}}$$

are the other five dimensionless parameters that appear in the nondimensionlized governing equations where ϕ_b and $\phi_{\rm np}$ represent the ratio of initial solute species concentration of fluid b and nanoparticles with respect to the initial solute species concentration of fluid a, respectively. There are 12 dimensional variables in a problem and these variables contain 4 fundamental dimensions—mass, length, time, and molar concentration of the solute—hence the nondimensional equations relating all the dimensional variables have a total of 8 dimensionless parameters.

According to the given diffusive characteristics scaling, the initial and the boundary conditions (6)–(12) are transformed as

$$\vec{u}(x, y, t = 0) = (1, 0), \tag{21}$$

$$(c_a, c_b, c_{\rm np})(x, y, t = 0) = (0, \phi_b, 0), \tag{22}$$

$$\vec{u}(x = 0, y, t) = (1, 0), \tag{23}$$

$$\vec{u}(x, y, t) = (1, 0) \quad \text{as} \quad x \to \infty, \tag{24}$$

$$(c_a, c_b, c_{\rm np})(x = 0, y, t) = (1, 0, \phi_{\rm np}), \tag{25}$$

$$\frac{\partial(c_a, c_b, c_{\rm np})}{\partial x} \to (0, 0, 0) \quad \text{as} \quad x \to \infty, \tag{26}$$

$$\frac{\partial(c_a, c_b, c_{\rm np})}{\partial y} \to (0, 0, 0), \qquad \frac{\partial v}{\partial y} \to 0 \quad \text{as} \quad y \to \pm\infty. \tag{27}$$

III. BASE-STATE SOLUTION

With the assumptions that there is no disturbance in the flow and diffusion of the species occurs only in the longitudinal direction, base-state equations are given as

$$\vec{u}^B = (1, 0), \tag{28}$$

$$\frac{dp^B}{dx} = -\mu^B, \tag{29}$$

$$\frac{\partial c_a^B}{\partial t} + \frac{\partial c_a^B}{\partial x} = \frac{\partial^2 c_a^B}{\partial x^2}, \tag{30}$$

$$\frac{\partial c_b^B}{\partial t} + \frac{\partial c_b^B}{\partial x} = \alpha_b \frac{\partial^2 c_b^B}{\partial x^2}, \tag{31}$$

$$\frac{\partial c_{\rm np}^B}{\partial t} + \frac{\partial c_{\rm np}^B}{\partial x} = \alpha_{\rm np}\frac{\partial^2 c_{\rm np}^B}{\partial x^2} - Da_{\rm dep}c_{\rm np}^B, \tag{32}$$

$$\mu_b = \mu_{\rm ref}e^{R_a c_a^B + R_b c_b^B + R_{\rm np}c_{\rm np}^B}, \tag{33}$$

where superscript B stands for the base-state variables. Accordingly, the boundary conditions for base-state concentrations are as follows:

$$c_a^B = 1, \quad c_b^B = 0, \quad c_{\rm np}^B = \phi_{\rm np} \quad \text{at} \quad x = 0, \tag{34}$$

$$\frac{\partial c_a^B}{\partial x} \to 0, \quad \frac{\partial c_b^B}{\partial x} \to 0, \quad \frac{\partial c_{\rm np}^B}{\partial x} \to 0 \quad \text{as} \quad x \to \infty, \tag{35}$$

and the initial condition for base-state concentrations is

$$c_a^B(x,0) = 0, \quad c_b^B(x,0) = \phi_b, \quad c_{\rm np}^B(x,0) = 0 \quad \forall x. \tag{36}$$

Base-state equations are linear in nature and their closed-form analytical solutions are attainable using the Laplace transform technique for a semi-infinite domain with the given boundary and initial conditions [32,33]. Thus, the closed-form solutions of base-state equations are given as [32,34]

$$c_a^B(x,t) = \left[\frac{1}{2}\text{erfc}\left(\frac{x-t}{2\sqrt{t}}\right) + \frac{e^x}{2}\ \text{erfc}\left(\frac{x+t}{2\sqrt{t}}\right)\right], \tag{37}$$

$$c_b^B(x,t) = \phi_b\left[1 - \frac{1}{2}\text{erfc}\left(\frac{x-t}{2\sqrt{\alpha_b t}}\right) - \frac{e^{(x/\alpha_b)}}{2}\ \text{erfc}\left(\frac{x+t}{2\sqrt{\alpha_b t}}\right)\right], \tag{38}$$

$$c_{\rm np}^B(x,t) = \phi_{\rm np}\left[\frac{e^{(1-w)x/2\alpha_{\rm np}}}{2}\text{erfc}\left(\frac{x-wt}{2\sqrt{\alpha_{\rm np} t}}\right) + \frac{e^{(1+w)x/2\alpha_{\rm np}}}{2}\ \text{erfc}\left(\frac{x+wt}{2\sqrt{\alpha_{\rm np} t}}\right)\right], \tag{39}$$

where $w = \sqrt{1 + 4Da_{\rm dep}\alpha_{\rm np}}$, $\text{erf}(x) = \frac{2}{\sqrt{\pi}}\int_0^x e^{-z^2}dz$, and $\text{erfc}(x) = 1 - \text{erf}(x)$.

Ghesmat *et al.* [7] determined the base-state solution in the form of a Fourier series using the separation of variables method. Moreover, the error in the solution has been reported later in an erratum [27]. Various inconsistencies are found in their determination of base-state solutions. Firstly, they assumed solution is separable in independent variables, and secondly, their solution is obtained by taking the periodic boundary conditions. Further, it is observed that their solutions suffer from oscillation due to the Gibbs phenomenon that occurs for jump discontinuity. As shown by Mojtabi and Deville [35], the analytical solution using the variable separable method of an advection-diffusion equation with Dirichlet homogeneous boundary conditions and an initial sine function becomes ill behaved when the advection becomes dominant. A comparison of the base-state concentration presented in this paper with the solution of Ghesmat *et al.* [7,27] is shown in Fig. 2, and it is clear that there is a significant difference between them. So in the subsequent study of this paper, nanoparticles impact on miscible VF has been studied using the more exact base-state solutions (37)–(39).

In our study, we have a total of eight nondimensional parameters, ϕ_b, α_b, $\phi_{\rm np}$, $\alpha_{\rm np}$, $Da_{\rm dep}$, R_a, R_b, and $R_{\rm np}$. The primary aim of our study is to analyze the impact of nanoparticles on the miscible VF. So, the value of parameters ϕ_b and α_b are assumed unity, corresponding to the miscible VF case without double-diffusivity effect between fluid a and fluid b. The addition of the nanoparticles cannot destabilize the nanoparticle free stable system [8,9], hence, we consider $R_a < R_b$ in the present study.

In the absence of deposition, a phase diagram of base-state viscosity at the initial time is shown in Fig. 3 in the plane of $(R, \alpha_{\rm np})$ where R is the effective log-mobility ratio defined as $R = \frac{R_{\rm np}\phi_{\rm np}}{R_b - R_a}$. It is clear that the parameters $R_a, R_b, \phi_{\rm np}, R_{\rm np}$ are linked together in R. Hence without loss of

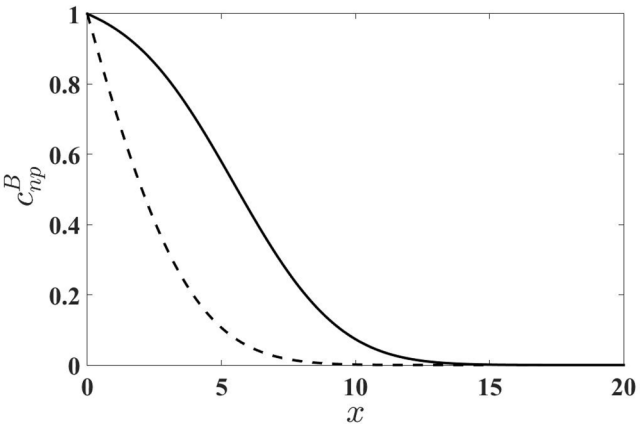

FIG. 2. Nanoparticles base concentration at time $t = 5$, where $\phi_{\rm np} = 1$, $\alpha_{\rm np} = 1$, and $Da_{\rm dep} = 0.02$. The solid line represents the base-state solution obtained in the present study and the dashed line represents the base-state series solution of Ghesmat *et al.* [7].

generality, the effect of R can be studied to bring the relevant effects on the dynamics of the instability. For the sake of clarity, we have fixed $\phi_{\rm np} = 1, R_a = 1, R_b = 4$ and R can be varied by changing $R_{\rm np}$. Thus, we are left with three nondimensional parameters $\alpha_{\rm np}$, R, and $Da_{\rm dep}$ whose effects on the dynamics of the problem has to be discussed. As clear in Fig. 3, the parameter space $(R, \alpha_{\rm np})$ is divided into six different regions depending on the base-state viscosity profile. As observed, the left-end base viscosity is less (more) than the right-end base viscosity for $R < 1$ ($R > 1$). The region $(R < 1, \alpha_{\rm np} < 1)$ is divided into region I and region II by finding the data points as fixing R with increasing $\alpha_{\rm np}$, such that the nonmonotonic viscosity profile becomes monotonic. Similarly, the region $(R > 1, \alpha_{\rm np} > 1)$ is divided into two regions, by finding the data points as fixing R with increasing $\alpha_{\rm np}$ such that the monotonic decreasing viscosity profile becomes nonmonotonic. These data points are shown as red dots in Fig. 3, and they follow the power rule $\alpha_{\rm np} \approx R^{2.15}$, which is obtained using the MATLAB tool box CFTOOL. It is observed that the base-state viscosity is monotonic in regions II, V and nonmonotonic in nature for regions I, III, IV, VI.

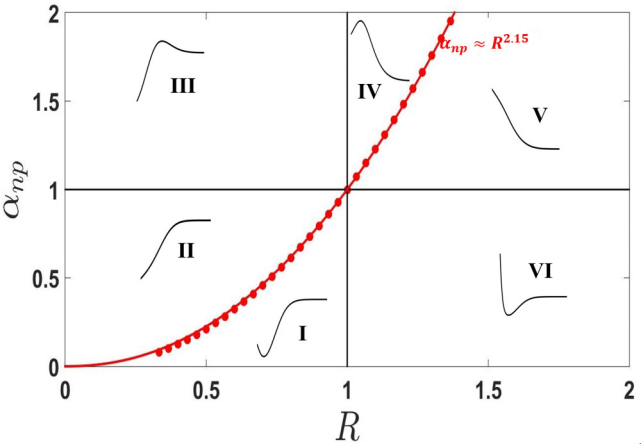

FIG. 3. Sketch of six different base-state viscosity profiles in the $(R, \alpha_{\rm np})$ plane at initial time $t = 0.01$ for $Da_{\rm dep} = 0$.

IV. LINEAR STABILITY ANALYSIS IN SELF-SIMILAR DOMAIN

Following the previous work [7,36,37], the linearized perturbed equations are obtained by introducing the infinitesimal perturbations around the base state as $f = f^B + \epsilon f^*$ where f^B in $\{u^B, c_a^B, c_b^B, c_{\rm np}^B\}$, f^* in $\{u^*, c_a^*, c_b^*, c_{\rm np}^*\}$ stands for base-state and perturbed quantities, respectively, with $\epsilon \ll 1$. Thus, the resulting coupled perturbed equations in the Eulerian frame are given as

$$\left[\frac{\partial^2}{\partial x^2} + \left(R_a\frac{\partial c_a^B}{\partial x} + R_b\frac{\partial c_b^B}{\partial x} + R_{\rm np}\frac{\partial c_{\rm np}^B}{\partial x}\right)\frac{\partial}{\partial x} + \frac{\partial^2}{\partial y^2}\right]u^* = -\left(R_a\frac{\partial^2 c_a^*}{\partial y^2} + R_b\frac{\partial^2 c_b^*}{\partial y^2} + R_{\rm np}\frac{\partial^2 c_{\rm np}^*}{\partial y^2}\right), \tag{40}$$

$$\left(\frac{\partial}{\partial t} + \frac{\partial}{\partial x} - \frac{\partial^2}{\partial x^2} - \frac{\partial^2}{\partial y^2}\right)c_a^* = -\frac{\partial c_a^B}{\partial x}u^*, \tag{41}$$

$$\left(\frac{\partial}{\partial t} + \frac{\partial}{\partial x} - \alpha_b\frac{\partial^2}{\partial x^2} - \alpha_b\frac{\partial^2}{\partial y^2}\right)c_b^* = -\frac{\partial c_b^B}{\partial x}u^*, \tag{42}$$

$$\left(\frac{\partial}{\partial t} + \frac{\partial}{\partial x} - \alpha_{\rm np}\frac{\partial^2}{\partial x^2} - \alpha_{\rm np}\frac{\partial^2}{\partial y^2} + Da_{\rm dep}\right)c_{\rm np}^* = -\frac{\partial c_{\rm np}^B}{\partial x}u^*. \tag{43}$$

Now, as the coefficients of the above equations are independent of y, further using the normal mode decomposition, the perturbations are decomposed along the y direction using $f^*(x, y, t) = f'(x, t)e^{iky}$. Thus, the resulting perturbed equations are transformed to

$$\left[\frac{\partial^2}{\partial x^2} + \left(R_a\frac{\partial c_a^B}{\partial x} + R_b\frac{\partial c_b^B}{\partial x} + R_{\rm np}\frac{\partial c_{\rm np}^B}{\partial x}\right)\frac{\partial}{\partial x} - k^2\right]u' = k^2\left(R_a c_a' + R_b c_b' + R_{\rm np}c_{\rm np}'\right), \tag{44}$$

$$\left(\frac{\partial}{\partial t} + \frac{\partial}{\partial x} - \frac{\partial^2}{\partial x^2} + k^2\right)c_a' = -\frac{\partial c_a^B}{\partial x}u', \tag{45}$$

$$\left(\frac{\partial}{\partial t} + \frac{\partial}{\partial x} - \alpha_b\frac{\partial^2}{\partial x^2} + \alpha_b k^2\right)c_b' = -\frac{\partial c_b^B}{\partial x}u', \tag{46}$$

$$\left(\frac{\partial}{\partial t} + \frac{\partial}{\partial x} - \alpha_{\rm np}\frac{\partial^2}{\partial x^2} + \alpha_{\rm np}k^2 + Da_{\rm dep}\right)c_{\rm np}' = -\frac{\partial c_{\rm np}^B}{\partial x}\,u', \tag{47}$$

where the perturbations decay to zero at both the longitudinal boundaries. Similarity transformation is often used due to the difficulty of localization of perturbation within the diffusive layer in the original perturbed system [4,38]. We also found a similar issue by solving Eqs. (44)–(47) numerically in the original coordinate system, not shown here for the sake of brevity. To overcome this difficulty, similarity transformation $\xi = \frac{x}{\sqrt{t}}$ [39] is used and the linearized perturbed equations (44)–(47) are transformed into

$$\left[\frac{\partial^2}{\partial \xi^2} + \left(R_a\frac{\partial c_a^B}{\partial \xi} + R_b\frac{\partial c_b^B}{\partial \xi} + R_{\rm np}\frac{\partial c_{\rm np}^B}{\partial \xi}\right)\frac{\partial}{\partial \xi} - k^2 t\right]u' = k^2 t\left(R_a c_a' + R_b c_b' + R_{\rm np}c_{\rm np}'\right), \tag{48}$$

$$\left(\frac{\partial}{\partial t} - \frac{\xi}{2t}\frac{\partial}{\partial \xi} + \frac{1}{\sqrt{t}}\frac{\partial}{\partial \xi} - \frac{1}{t}\frac{\partial^2}{\partial \xi^2} + k^2\right)c_a' = -\frac{1}{\sqrt{t}}\frac{\partial c_a^B}{\partial \xi}\,u', \tag{49}$$

$$\left(\frac{\partial}{\partial t} - \frac{\xi}{2t}\frac{\partial}{\partial \xi} + \frac{1}{\sqrt{t}}\frac{\partial}{\partial \xi} - \frac{\alpha_b}{t}\frac{\partial^2}{\partial \xi^2} + \alpha_b k^2\right)c_b' = -\frac{1}{\sqrt{t}}\frac{\partial c_b^B}{\partial \xi}u', \tag{50}$$

$$\left(\frac{\partial}{\partial t} - \frac{\xi}{2t}\frac{\partial}{\partial \xi} + \frac{1}{\sqrt{t}}\frac{\partial}{\partial \xi} - \frac{\alpha_{\rm np}}{t}\frac{\partial^2}{\partial \xi^2} + \alpha_{\rm np}k^2 + Da_{\rm dep}\right)c_{\rm np}' = -\frac{1}{\sqrt{t}}\frac{\partial c_{\rm np}^B}{\partial \xi}u' \tag{51}$$

with the decaying boundary condition at both the inlet and the outlet boundary. Further, as the time t appears in the denominator, so as to remove the singularity in the obtained differential equations, the initial time for numerical simulation is assumed to be $t_0 = 10^{-4}$.

The computational domain $\xi \in [0, L]$ has been discretized into $n+2$ grid points with spacing size h. By applying the central finite-difference discretization scheme, the coupled system of equations (48)–(51) can be recast as

$$M_1 U' = M_2 C'_a + M_3 C'_b + M_4 C'_{\rm np}, \tag{52}$$

$$\frac{dC'_a}{dt} + M_5 C'_a = M_6 U', \tag{53}$$

$$\frac{dC'_b}{dt} + M_7 C'_b = M_8 U', \tag{54}$$

$$\frac{dC'_{\rm np}}{dt} + M_9 C'_{\rm np} = M_{10} U', \tag{55}$$

where each matrix M_1 to M_{10} is of order $n \times n$ (matrix expressions are shown in Appendix A) and the unknown vectors are

$$C'_a = \begin{bmatrix} c'_a(h,t) \\ c'_a(2h,t) \\ \cdot \\ \cdot \\ \cdot \\ c'_a(nh,t) \end{bmatrix}, \quad C'_b = \begin{bmatrix} c'_b(h,t) \\ c'_b(2h,t) \\ \cdot \\ \cdot \\ \cdot \\ c'_b(nh,t) \end{bmatrix}, \quad C'_{\rm np} = \begin{bmatrix} c'_{\rm np}(h,t) \\ c'_{\rm np}(2h,t) \\ \cdot \\ \cdot \\ \cdot \\ c'_{\rm np}(nh,t) \end{bmatrix}, \quad \text{and} \quad U' = \begin{bmatrix} u'(h,t) \\ u'(2h,t) \\ \cdot \\ \cdot \\ \cdot \\ u'(nh,t) \end{bmatrix}.$$

Now by eliminating U' from the above set of equations, we can recast the problem as an IVP in the matrix form as

$$\frac{d}{dt}\begin{bmatrix} C'_a \\ C'_b \\ C'_{\rm np} \end{bmatrix} = \begin{bmatrix} M_6 M_1^{-1} M_2 - M_5 & M_6 M_1^{-1} M_3 & M_6 M_1^{-1} M_4 \\ M_8 M_1^{-1} M_2 & M_8 M_1^{-1} M_3 - M_7 & M_8 M_1^{-1} M_4 \\ M_{10} M_1^{-1} M_2 & M_{10} M_1^{-1} M_3 & M_{10} M_1^{-1} M_4 - M_9 \end{bmatrix} \begin{bmatrix} C'_a \\ C'_b \\ C'_{\rm np} \end{bmatrix} \tag{56}$$

with a random initial condition of infinitesimal small amplitude a for LSA. Following the previous studies [38], IVP is solved numerically using the explicit Runge-Kutta method with MATLAB in-built function ODE45.

Here, we used the two-norm for the energy calculation of the perturbations and evolved base state, and defined it as

$$E'(t) = (\|c'_a(x,t)\|_2)^2 + (\|c'_b(x,t)\|_2)^2 + (\|c'_{\rm np}(x,t)\|_2)^2 + (\|\vec{u}'(x,t)\|_2)^2, \tag{57}$$

$$E^B(t) = \left(\left\|c^B_a(x,t)\right\|_2\right)^2 + \left(\left\|c^B_b(x,t)\right\|_2\right)^2 + \left(\left\|c^B_{\rm np}(x,t)\right\|_2\right)^2 + \left(\left\|\vec{u}^B(x,t)\right\|_2\right)^2. \tag{58}$$

When the base state is time dependent, the growth rate of the perturbation is measured with respect to the growth of the evolved base state. In order to characterize the stability analysis, the instantaneous growth rate of perturbations (σ) is defined as [38,40]

$$\sigma(t) = \sigma'(t) - \sigma_b(t) = \frac{1}{E'}\frac{dE'}{dt} - \frac{1}{E^B}\frac{dE^B}{dt}, \tag{59}$$

where $\sigma > 0$ and $\sigma < 0$ characterize the stable and the unstable region, respectively.

It is observed that the growth rate is accurate up to the order of 10^{-2} for any values of parameters, when the length of the domain is more than 50 (see Fig. 4 when $R = 3, k = 0.2$). Hence, $L = 50$ is assumed in our study for time-efficient study. In a similar way, the obtained IVP is solved with different domain length, step size, and amplitude of perturbations for a convergence study of the solution, and we found that $L = 50$, $h = 0.5$, and $a = 10^{-5}$ are sufficient for the time-efficient and optimal solution.

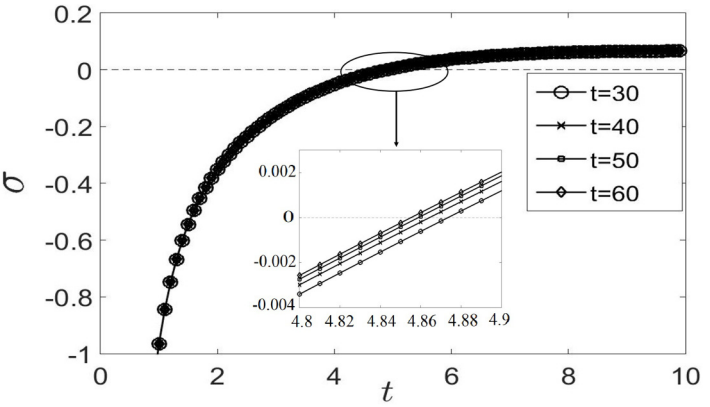

FIG. 4. Dependence on the domain length L on the growth rate using SSIVP, for $R = 3, k = 0.2$.

Following the studies of IVP analysis with the absorbing inlet boundary condition [4,41], we defined the dominating eigenmode as the initial condition of the given IVP by

$$(c_a', c_b', c_{\rm np}')(\xi, t_0) = \left[\xi \exp\left(-\frac{\xi^2}{4}\right), \xi \exp\left(-\frac{\xi^2}{4}\right), \xi \exp\left(-\frac{\xi^2}{4}\right)\right] \tag{60}$$

and found that the growth rate obtained using the dominant eigenmode is in line with the growth rate obtained using the averaging of the random initial conditions for all time $t > O(10^{-1})$, not shown here for sake of brevity. So for the time-efficient study, we numerically solve the IVP [Eq. (56)] using the dominant eigenmode in the subsequent study.

V. RESULTS AND DISCUSSION

All the available literature of nanoparticles impact on miscible VF is performed under the QSSA [7–9]. Ghesmat *et al.* [7] performed their study for absorbing the inlet boundary condition by freezing the base-state time $t = 5$, whereas Dastvareh and Azaiez [8] and Sabet *et al.* [9] reported their results for the reflective inlet boundary. In the study of Dastvareh and Azaiez [8], the instability growth rate is calculated by freezing the base-state time at $t = 1$. Later, Sabet *et al.* [9] reported that problem is sensitive to base-state freezing time to analyze the dynamics of the problem. Further, previous studies show (see Fig. 7 of [9]) that system having $R_a = 1, R_b = 4, R_{\rm np} = 1, Da_{\rm dep} = 0, \alpha_{\rm np} = 2$ is unconditionally unstable for the initial period of time. But physically, the system has to be stable due to the dominance of diffusion forces over convection in the initial period of time [38,42]. So nonmodal analysis using IVP in the self-similar domain is used to discuss the early time dynamics of nanoparticles on miscible VF more accurately in the subsequent study.

The neutral stability curve (i.e., $\sigma = 0$ isocontour) in the parameter space (k, t) is plotted where the region below and above the $\sigma = 0$ isocontour curve corresponds to stable ($\sigma < 0$) and unstable regions ($\sigma > 0$), respectively. Neutral stability curves are shown in Fig. 5, for different values of $\alpha_{\rm np}$ in the absence of deposition of nanoparticles at $R_{\rm np} = 4$, i.e., $R = 1.33$. It is observed that in the instability region, the time as well as the wave-number ranges, shrinks more for $\alpha_{\rm np} = 1.5$ than for $\alpha_{\rm np} = 0.4$ and $\alpha_{\rm np} = 3$. As shown in Fig. 3, $\alpha_{\rm np} = 0.4,\ 1.5,$ and 3 for $R = 1.33$ corresponds to region VI, region V, and region IV, respectively. Since, the base-viscosity profile in region V is monotonic decreasing, whereas in regions IV and VI it is nonmonotonic, as expected region V is less unstable than region IV and region VI.

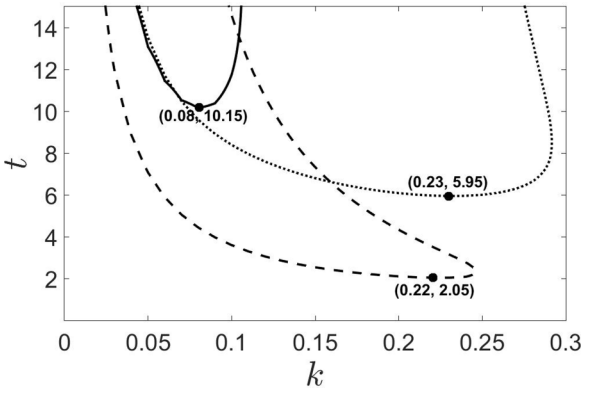

FIG. 5. Neutral stability curve using IVP in the (ξ, t) domain at $R = 1.33$, $Da_{\text{dep}} = 0$ where the dashed curve, solid curve, and dotted curve correspond to $\alpha_{\text{np}} = 0.4$, $\alpha_{\text{np}} = 1.5$, and $\alpha_{\text{np}} = 3$, respectively. The solid dot on the curve stands for the corresponding critical point.

Here, the lowest point of the $\sigma = 0$ isocontour corresponds to the critical time (t_c) and critical wave number (k_c), which can be defined as follows:

$$t_c(R, \alpha_{\text{np}}, Da_{\text{dep}}) := \min_t\{t : \sigma(t, k, R, \alpha_{\text{np}}, Da_{\text{dep}}) \geqslant 0\}, \tag{61}$$

$$k_c(R, \alpha_{\text{np}}, Da_{\text{dep}}) := \min_k\{k : \sigma(t_c, k, R, \alpha_{\text{np}}, Da_{\text{dep}}) = 0\}. \tag{62}$$

Further, we define the maximum growth rate (σ_m) of the perturbation for all possible wave numbers k with a frozen time as follows:

$$\sigma_m(t, R, \alpha_{\text{np}}, Da_{\text{dep}}) := \max_k\{\sigma(k, t, \alpha_{\text{np}}, R, Da_{\text{dep}})\}. \tag{63}$$

In Fig. 6, we plotted σ_m as a function of time t for different α_{np}. We define the onset time of instability t_c as the instant of time when $\sigma_m(t)$ becomes negative to positive. A shorter t_c referred to an early onset of instability, whereas a larger t_c referred to the delay in the onset of instability. From Fig. 6, it is clearly depicted that the onset time t_c as well as σ_m behaves nonmonotonically as a function of α_{np}.

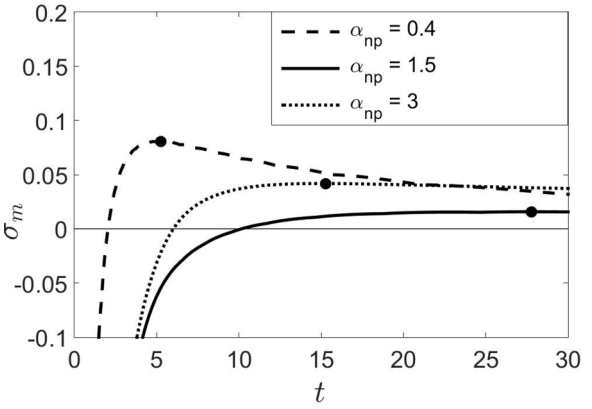

FIG. 6. Instantaneous maximum growth rate (σ_m) as a function of t for $R = 1.33$, $Da_{\text{dep}} = 0$ at different α_{np} values, where the dot in the curve corresponds to the maximum growth rate.

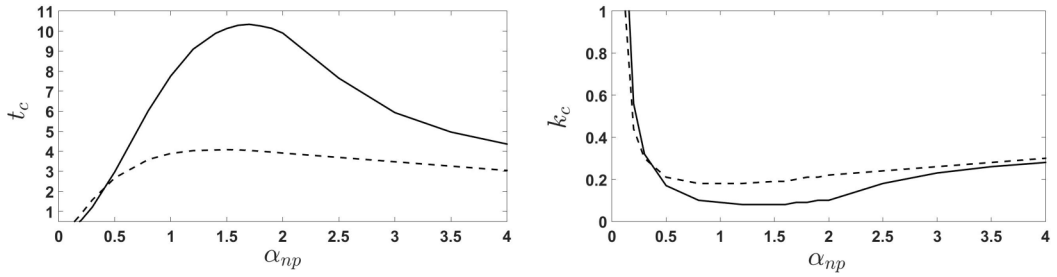

FIG. 7. (a) Critical time and (b) critical wave number as a function of $\alpha_{\rm np}$ for $Da_{\rm dep} = 0$ where the solid line and the dashed line stand for $R = 1.33$ and $R = 0.66$, respectively.

As t_c is the onset time of instability for all possible wave numbers, it is more instructive to determine how a physical system behaves to any physical perturbations present in the system. Hence in the subsequent study, t_c as a function of $\alpha_{\rm np}$, R, $Da_{\rm dep}$ is used to study the influence of nanoparticles on miscible VF. Ghesmat *et al.* [7] and Dastvareh and Azaiez [8] studied the influence of nanoparticles in the presence of the deposition of nanoparticles, whereas Sabet *et al.* [9] studies the nanoparticles impact in depositing as well as in nondepositing of nanoparticles, as nanoparticles deposition in porous media can occur or be avoided using many technologies [26]. We divided the study into two general cases: (i) the absence of the deposition of nanoparticles ($Da_{\rm dep} = 0$) and (ii) the presence of the deposition of nanoparticles ($Da_{\rm dep} \neq 0$).

A. Absence of the deposition of nanoparticles

1. Effect of α_{np}

In absence of the deposition, t_c and k_c are plotted as a function of $\alpha_{\rm np}$ for $R_{\rm np} = 2$ ($R = 0.66$) and $R_{\rm np} = 4$ ($R = 1.33$) (see Fig. 7). Our finding suggests that both the onset time of the instability and the critical wave number are nonmonotonic functions of $\alpha_{\rm np}$ for $R < 1$ and $R > 1$. Unimodal distribution of the onset time as a function of $\alpha_{\rm np}$ is obtained where the peak is observed approximately in the middle range of $\alpha_{\rm np} \in (1, 2)$. Thus initially, instability decreases with increasing $\alpha_{\rm np}$, and then instability increases with the further increase of $\alpha_{\rm np}$. Such effect of $\alpha_{\rm np}$ on the instability at $Da_{\rm dep} = 0$ is in line with the results of Ghesmat *et al.* [7] and Sabet *et al.* [9]. Further, the detailed analysis using the maximum growth rate over all time $\sigma_{\rm max}$ is discussed in Appendix B with the corresponding effects of $\alpha_{\rm np}$. Interestingly we find the nonmonotonic behavior of $\sigma_{\rm max}$ versus $\alpha_{\rm np}$ and the corresponding critical time and wave-number explanations remain unchanged qualitatively to the results obtained in the explanation of t_c with respect to $\alpha_{\rm np}$.

As shown in Fig. 3, the base-state viscosity profile changes its behavior with increasing $\alpha_{\rm np}$ for $R < 1$ as well as for $R > 1$. For $R < 1$, a favorable viscosity gradient plays an important role, and it is clear from Fig. 8(a) that a favorable viscosity gradient for instability is more for region I and region III than region II. Hence, region II is less stable than region I and region III. Therefore, t_c is a nonmonotonic function of $\alpha_{\rm np}$ for $R < 1$. Further, it is clear from Fig. 8(b) that region V is more stable than region VI and region IV, so t_c is more for the middle range of $\alpha_{\rm np}$ than for other $\alpha_{\rm np}$ values for $R > 1$.

2. Effect of R

In the absence of the deposition of nanoparticles, t_c is monotonically increasing with increasing R for $\alpha_{\rm np} = 1.5$ and $\alpha_{\rm np} = 4$, whereas t_c is monotonically decreasing with increasing R for $\alpha_{\rm np} = 0.2$ (see Fig. 9). Further, the results indicate that t_c grows more rapidly for $\alpha_{\rm np} = 1.5$ than for $\alpha_{\rm np} = 4$.

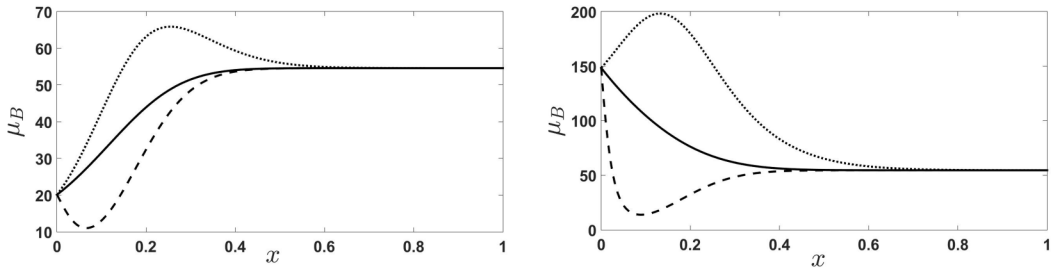

FIG. 8. Base-state viscosity profile (a) $R < 1$ and (b) $R > 1$ at $t = 0.01$ in the absence of deposition where the dashed, solid, and dotted curves stand for $\alpha_{np} = 0.3$, $\alpha_{np} = 1$, and $\alpha_{np} = 4$, respectively.

B. Presence of the deposition of nanoparticles

Critical time as a function of the deposition rate of nanoparticles (Da_{dep}) is plotted for different values of R and α_{np}. A unimodal distribution of onset time as a function of Da_{dep} is obtained for $\alpha_{np} = 0.2$, where the peak is observed approximately at $Da_{dep} = 0.5$ [see Fig. 10(a)]. Whereas Figs. 10(b) and 10(c) show that t_c is a decreasing function of Da_{dep} for $\alpha_{np} = 1.5$ and $\alpha_{np} = 4$. In contrast, previous studies [7–9,16] reported that the nanoparticles deposition rate has only a destabilized effect on the VF instability.

For $\alpha_{np} = 0.2$, two types of base-state viscosity profiles exist with time for $R = 0.66$ as well as for $R = 1.33$ (see Fig. 11). Profile (ii) is more unstable than profile (i) since there are two favorable viscosity gradients for instability appearing in profile (ii), whereas only one favorable viscosity gradient appears in profile (i). In addition, it is observed that the time range of appearance in profile (ii) decreases with increasing Da_{dep}, whereas the favorable viscosity gradient for instability increases with increasing Da_{dep}. For the smaller value of $Da_{dep} \lesssim O(10^{-1})$, instability behavior is dominated only by the viscosity profile (ii) type, which diminished with increased Da_{dep}, hence the onset time of instability increases with increasing Da_{dep}. Whereas for $Da_{dep} \gtrsim O(1)$, profile (ii) appears for an infinitesimally short time, and hence the favorable viscosity gradient dominates the instability, which increases with the increase of Da_{dep}. Hence, the onset time t_c becomes a decreasing function of Da_{dep}. Thus, t_c behaves nonmonotonically as a function of Da_{dep} for $\alpha_{np} = 0.2$.

As for $\alpha_{np} = 0.2$, $Da_{dep} \lesssim O(10^{-1})$, instability behavior is dominated only by the viscosity profile (ii), and the favorable viscosity gradient of instability is more for $R = 1.33$ as compared to $R = 0.66$. Hence, $t_c(R = 1.33) < t_c(R = 0.66)$ for smaller values of Da_{dep}. But for larger values

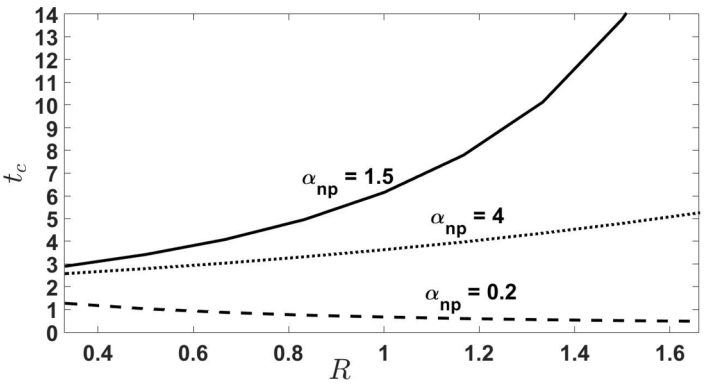

FIG. 9. Critical time t_c as a function of R when $Da_{dep} = 0$.

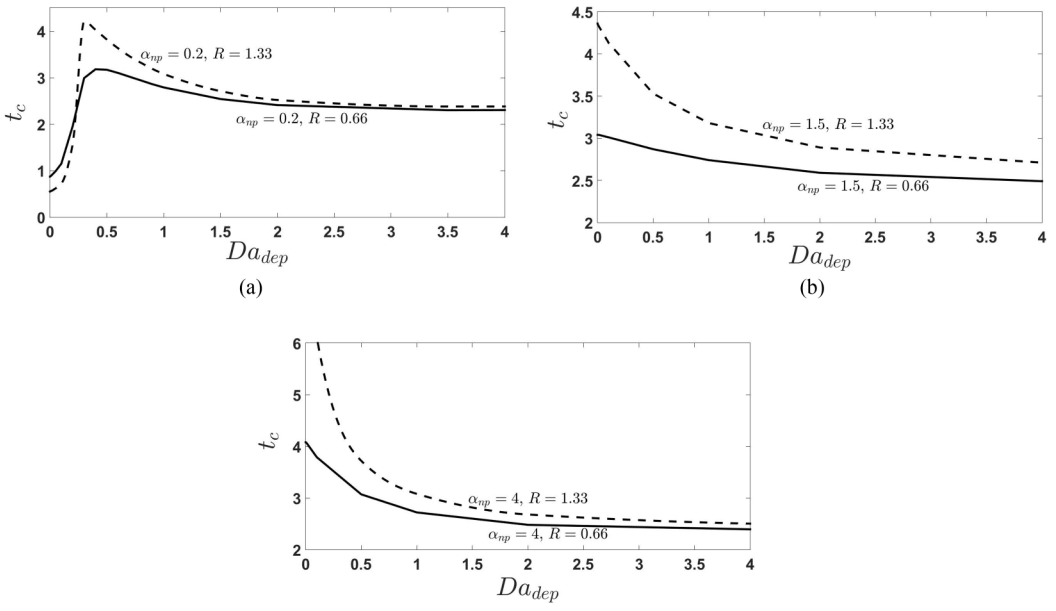

FIG. 10. Critical time as a function of Da_{dep} for (a) $\alpha_{\text{np}} = 0.2$, (b) $\alpha_{\text{np}} = 1.5$, and (c) $\alpha_{\text{np}} = 4$, where the solid line and the dashed line stand for $R = 0.66$ and $R = 1.33$, respectively.

of $Da_{\text{dep}} \gtrsim O(1)$, instability behavior is dominated only by the viscosity profile (i), and unfavorable viscosity gradient for instability at the inlet increases with increasing R. Hence, the instability decreases with increasing R; $t_c(R = 1.33) > t_c(R = 0.66)$ for larger values of Da_{dep}; and the crossover of the $R < 1$ and $R > 1$ curves appears for the onset t_c as a function of Da_{dep}. Although when $Da_{\text{dep}} \gtrsim O(10)$, nanoparticles deposit completely on the inlet boundary in infinitesimal small time, thus the effect of nanoparticles is negligible, so t_c values are approximately the same for every R_{np} and α_{np}.

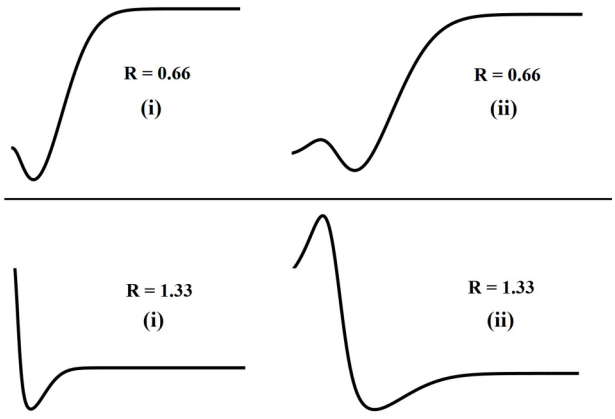

FIG. 11. Different types of base-state viscosity profiles appear with time when $\alpha_{\text{np}} = 0.2$ where the first row is for $R = 0.66$ and the second row is for $R = 1.33$.

For $\alpha_{np} > 1$, it is observed that favorable viscosity gradient for instability is more and unfavorable viscosity gradient for instability is less for $R < 1$ (region III in Fig. 3) as compared to $R > 1$ (region IV and region V in Fig. 3) for all Da_{dep}, so the onset time is less for $R = 0.66$ as compared to $R = 1.33$ at $\alpha_{np} = 1.5$ and $\alpha_{np} = 4$ for all Da_{dep}. In addition, our result indicates that t_c is a decreasing function of Da_{dep} for $\alpha_{np} > 1$ for all R.

From Fig. 10, it is also clear that in the absence of the deposition of nanoparticles (i.e., $Da_{dep} = 0$), the onset time is a decreasing function of R for $\alpha_{np} = 0.2$ and an increasing function of R for $\alpha_{np} = 1.5$ and $\alpha_{np} = 4$ (as shown in Fig. 9). In addition, our results indicate that t_c is an increasing function of R for $\alpha_{np} = 0.2,\ 1.5,$ and 4 when $Da_{dep} \gtrsim O(1)$. Whereas, previous studies [7–9] reported that instability decreases with increasing R for all values of α_{np} and Da_{dep}.

As shown in Fig. 10, t_c is more for $R = 0.66$ than for $R = 1.33$ at $\alpha_{np} = 0.2$ when $Da_{dep} = 0$, whereas t_c is less for $R = 0.66$ than for $R = 1.33$ at $\alpha_{np} = 1.5$ and 4 when $Da_{dep} = 0$. Hence, the crossing of the curves appears in Fig. 7(a). Further, our findings suggest that onset time increases with increasing α_{np} for $R < 1$ as well as for $R > 1$ when $Da_{dep} \gtrsim O(1)$, whereas t_c is a nonmonotonic function of α_{np} for $R < 1$ as well as for $R > 1$ when $Da_{dep} \lesssim O(10^{-1})$.

VI. NONLINEAR SIMULATIONS

Finite element simulations using COMSOL MULTIPHYSICS [43] is used for nonlinear analysis. Various COMSOL models are available in literature for miscible VF. Van Dam *et al.* [44] performed an analysis by coupling of the "Darcy's law (dl)" model and the "transport of dilute species in porous media (tds)" model. Whereas, Sharma *et al.* [45] used the "Two-Phase Darcy's Law (TPDL)" model of the fluid flow module. In the present work, we use four physics interfaces of COMSOL to solve the nonlinear coupled dimensionless equations (15)–(20). "Darcy's law (dl)" is used for fluid flow and "transport of diluted species in porous media (tds)" is used to model the transport of solute concentrations c_a, c_b, and c_{np}. By setting the value of porosity (ϵ_p) and permeability of the medium (κ) to be unity, the DL-model equations of COMSOL MULTIPHYSICS reduce to Eqs. (15) and (16). Species concentration equations (17), (18), and (19) obtained from the tds model of COMSOL MULTIPHYSICS by setting the reaction term R_i as 0, 0, and $-Da_{dep}c_{np}$, respectively. Further, the velocity field in the tds model is selected as "Darcy's velocity field (dl)." Viscosity in the dl model is set as $\mu = e^{R_a c_a + R_b c_b + R_{np} c_{np}}$ to model Eq. (20).

Further, initial and boundary conditions (21)–(27) are modeled in COMSOL. In the dl model of COMSOL, the inlet and outlet boundary conditions for fluid velocity are fixed to $\vec{u} = (1, 0)$ and $p = 0$, respectively. In addition, the initial condition in the dl model of COMSOL is given as $p = 0$, which is equivalent to $\vec{u}(x, y, 0) = (1, 0)$. At transverse boundaries, no flow boundary conditions are implemented. For concentration, no flux conditions are specified at the transverse boundaries and outlet of domain in the tds model of COMSOL. Further, the initial conditions of concentrations are set as $(c_a, c_b, c_{np}) = (0, \phi_b, 0)$. Boundary conditions at the inlet are set as $c_a = 1$, $c_{np} = \phi_{np}$. We used the mapped mesh discretization for numerical simulation in COMSOL. As the mapped mesh is structured meshing, there is no perturbation at the interface, so only diffusion at the interface is observed. For inserting perturbation in the system, we used the inlet boundary condition for concentration c_b as

$$c_b(0, y, t) = \begin{cases} |rn1(y)| : t = 0 \\ 0 : t > 0, \end{cases} \tag{64}$$

where $rn1(y)$ is a COMSOL in-built random function having uniform distribution and the amplitude of $rn1(y)$ is assumed of order $O(10^{-3})$. The MUMPS numerical time-dependent solver of COMSOL is used for numerical simulations of the proposed problem. In present work, the length ($L = 3000$) and width ($W = 500$) of the domain are assumed for the numerical solution. Further, a mapped mesh is used with the step size $(\Delta x, \Delta y) = (5, 5)$. A convergence study for $(L, W, \Delta x, \Delta y)$ is also performed such that the results are qualitatively invariant.

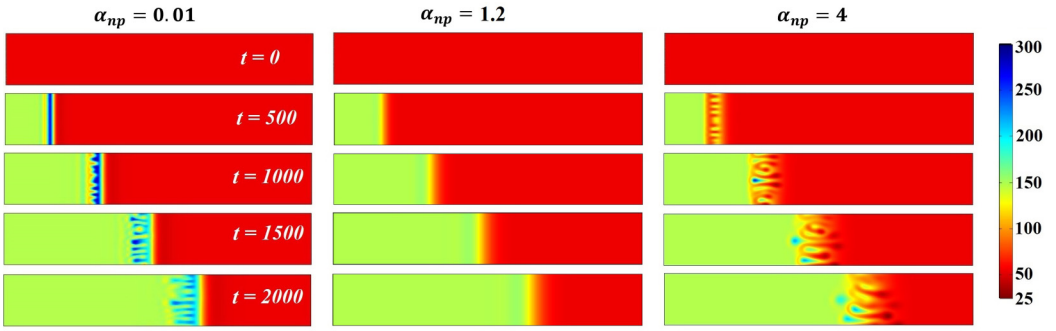

FIG. 12. Viscosity density plot at successive times $t = 0, 500, 1000, 1500, 2000$ (from top to bottom) for $R = 1.33$, $Da_{\text{dep}} = 0$ where $\alpha_{\text{np}} = 0.01, 1.2, 4$ increases from left to right.

Density plots of the viscosity profile are depicted in Fig. 12 for different values of α_{np} with $R = 1.33$ and $Da_{\text{dep}} = 0$. It is clearly observed that at $t = 500$ for $\alpha_{\text{np}} = 4$ instability appears, whereas there is no instability seen for a large time even up to $t = 2000$ when $\alpha_{\text{np}} = 1.2$. For smaller $\alpha_{\text{np}} = 0.01$, instability occurs approximately when $t = 1000$. This shows the nonmonotonic nature of the onset of instability with respect to the values α_{np}. This result verifies the nonmonotonic nature of t_c as a function of α_{np} obtained from LSA [see Figs. 5 and 7(a)]. Also for smaller values of α_{np}, backward finger dynamics are observed due to the dominance of viscosity profile type (ii) (see Fig. 11) at $R = 1.33$, $\alpha_{\text{np}} < O(10^{-1})$.

VII. CONCLUSION

Our study considered the flow configuration such that less viscous fluid-carrying nanoparticles displace a more viscous fluid through the inlet boundary [7]. A more accurate exact solution of the base state is described utilizing the Laplace transform, and LSA is performed using the IVP in the self-similar domain to get the onset time more accurately. We studied the effect of nanoparticles on instability using the critical time t_c as a function of α_{np}, R, Da_{dep}. The present results in our analysis can be summarized as follows: For smaller values of $Da_{\text{dep}} \lesssim O(10^{-1})$, initially VF instability decreases with increasing α_{np} up to the turning point of approximately 1.5 and then instability increases with further increasing of α_{np}, whereas instability decreases with increasing α_{np} for all values of R when $Da_{\text{dep}} \gtrsim O(1)$. Our finding suggests that VF instability decreases with increasing R for all values of α_{np} when $Da_{\text{dep}} \gtrsim O(1)$. While for smaller values of $Da_{\text{dep}} \lesssim O(10^{-1})$, instability decreases with increasing R for $\alpha_{\text{np}} > 1$, whereas instability increases with increasing R for small values of $\alpha_{\text{np}} \lesssim O(10^{-1})$. Further, VF instability increases with increasing Da_{dep} for all values of R when $\alpha_{\text{np}} > 1$. Although for smaller values of $\alpha_{\text{np}} \lesssim 1$, instability decreases with increasing Da_{dep} up to a turning point and then instability decreases with increasing Da_{dep}. Further, results obtained from the LSA are compared with the COMSOL numerical simulations, and outcomes are found in very good agreement. Our study removes the various inconsistencies available in the literature since LSA was performed using QSSA in the literature [7–9]. These results provide a basis for controlling VF instability using nanofluid displacement processes, such as nanoparticle-based drug delivery, and soil and groundwater remediation by delivering the fluid-carrying nanoparticles to *in situ* contaminated areas [46].

ACKNOWLEDGMENT

M.M. acknowledges the financial support from SERB, Government of India through Grant No. CRG/2020/000613 and SPARC, Government of India through Grant No. SPARC/2018-2019/P450/SL.

APPENDIX A: MATRIX EXPRESSIONS

The matrices M_1 to M_{10} of order $n \times n$ are given as

$$M_1(i,j) = \begin{cases} \frac{1}{h^2} \pm \frac{\{R_a[c_a^B(i+2) - c_a^B(i)] + R_b[c_b^B(i+2) - c_b^B(i)] + R_{\rm np}[c_{\rm np}^B(i+2) - c_{\rm np}^B(i)]\}}{4h^2} & \text{if } i \pm 1 = j \\ -\frac{2}{h^2} - k^2 t & \text{if } i = j \\ 0 & \text{otherwise,} \end{cases}$$

$$M_2(i,j) = \begin{cases} k^2 t R_a & \text{if } i = j \\ 0 & \text{otherwise,} \end{cases}$$

$$M_3(i,j) = \begin{cases} k^2 t R_b & \text{if } i = j \\ 0 & \text{otherwise,} \end{cases}$$

$$M_4(i,j) = \begin{cases} k^2 t R_{\rm np} & \text{if } i = j \\ 0 & \text{otherwise,} \end{cases}$$

$$M_5(i,j) = \begin{cases} -\frac{1}{h^2 t} \mp \frac{\xi(ii+1)}{4ht} \pm \frac{1}{2h\sqrt{t}} & \text{if } i = j \pm 1 \\ \frac{2}{h^2 t} + k^2 & \text{if } i = j \\ 0 & \text{otherwise,} \end{cases}$$

$$M_7(i,j) = \begin{cases} -\frac{\alpha_b}{h^2 t} \mp \frac{\xi(ii+1)}{4ht} \pm \frac{1}{2h\sqrt{t}} & \text{if } i = j \pm 1 \\ \frac{2\alpha_b}{h^2 t} + k^2 & \text{if } i = j \\ 0 & \text{otherwise,} \end{cases}$$

$$M_9(i,j) = \begin{cases} -\frac{\alpha_{\rm np}}{h^2 t} \mp \frac{\xi(ii+1)}{4ht} \pm \frac{1}{2h\sqrt{t}} & \text{if } i = j \pm 1 \\ \frac{2\alpha_{\rm np}}{h^2 t} + k^2 + Da_{\rm dep} & \text{if } i = j \\ 0 & \text{otherwise,} \end{cases}$$

$$M_6(i,j) = \begin{cases} \frac{c_a^B(i) - c_a^B(i+2)}{2h\sqrt{t}} & \text{if } i = j \\ 0 & \text{otherwise,} \end{cases}$$

$$M_8(i,j) = \begin{cases} \frac{c_b^B(i) - c_b^B(i+2)}{2h\sqrt{t}} & \text{if } i = j \\ 0 & \text{otherwise,} \end{cases}$$

$$M_{10}(i,j) = \begin{cases} \frac{c_{\rm np}^B(i) - c_{\rm np}^B(i+2)}{2h\sqrt{t}} & \text{if } i = j \\ 0 & \text{otherwise,} \end{cases}$$

where $i \in \{1, 2, 3, \ldots, n\}$, $j \in \{1, 2, 3, \ldots, n\}$. It is clear that M_1, M_5, M_7, M_9 are the tridiagonal matrices and others are the diagonal matrices.

APPENDIX B: MAXIMUM GROWTH RATE

The maximum growth rate ($\sigma_{\max}$) is defined as the maximum of σ_m over time as follows:

$$\sigma_{\max}(R, \alpha_{\rm np}, Da_{\rm dep}) := \max_t \{\sigma_m(t, \alpha_{\rm np}, R, Da_{\rm dep})\}, \tag{B1}$$

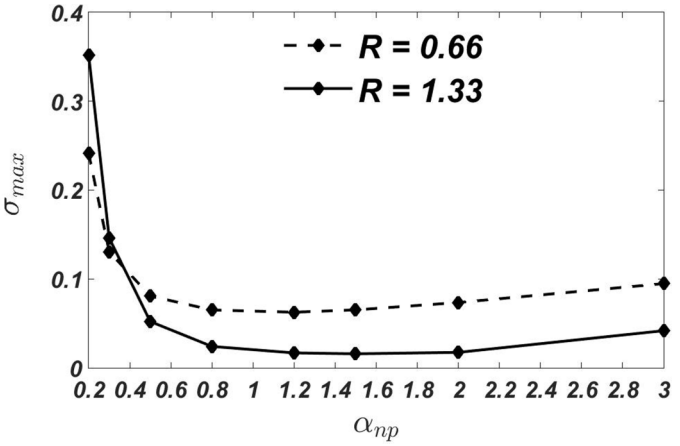

FIG. 13. Maximum growth rate ($\sigma_{\max}$) as a function of $\alpha_{\rm np}$ for $Da_{\rm dep} = 0$, where the solid and dashed curves stand for $R = 1.33$ and $R = 0.66$, respectively.

and corresponding critical time ($t_{\rm crit}$) and critical wave number ($k_{\rm crit}$) with respect to the maximum growth rate can be defined as follows:

$$t_{\rm crit}(R, \alpha_{\rm np}, Da_{\rm dep}) := \{t : \sigma_m(t, R, \alpha_{\rm np}, Da_{\rm dep}) = \sigma_{\max}(R, \alpha_{\rm np}, Da_{\rm dep})\}, \tag{B2}$$

$$k_{\rm crit}(R, \alpha_{\rm np}, Da_{\rm dep}) := \{k : \sigma(k, t_{\rm crit}, R, \alpha_{\rm np}, Da_{\rm dep}) = \sigma_m(t_{\rm crit}, R, \alpha_{\rm np}, Da_{\rm dep})\}. \tag{B3}$$

In Fig. 13, we plotted $\sigma_{\max}$ as a function of $\alpha_{\rm np}$ for $Da_{\rm dep} = 0$ at $R = 0.66, 1.33$. It is clear that $\sigma_{\max}$ first decreases and then increases with $\alpha_{\rm np}$ for both $R = 1.33$ and $R = 0.66$. Thus initially, instability decreases with increasing $\alpha_{\rm np}$, and then instability increases with the further increase of $\alpha_{\rm np}$. Such effect of $\alpha_{\rm np}$ on the instability is in line with the results presented using t_c in our study (see Fig. 7). Therefore we find that the early onset gives rise to a more unstable flow and delay onset corresponds to less unstable flow. Further, in Fig. 14, the critical time and critical wave number corresponding to $\sigma_{\max}$ are plotted, and show the same qualitative analysis as t_c and k_c in Fig. 7.

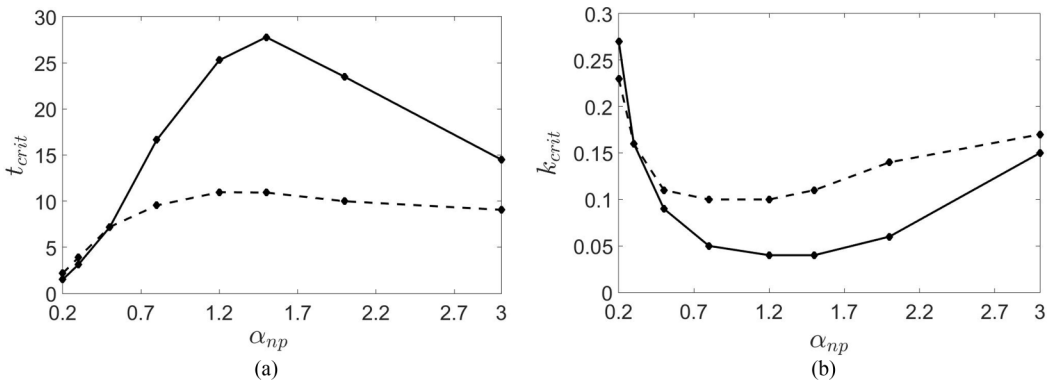

FIG. 14. (a) Critical time ($t_{\rm crit}$) and (b) critical wave number ($k_{\rm crit}$) as a function of $\alpha_{\rm np}$ for $Da_{\rm dep} = 0$, where the solid and dashed curves stand for $R = 1.33$ and $R = 0.66$, respectively.

[1] P. G. Saffman and G. I. Taylor, The penetration of a fluid into a porous medium or Hele-Shaw cell containing a more viscous liquid, Proc. R. Soc. London, Ser. A **245**, 312 (1958).
[2] G. M. Homsy, Viscous fingering in porous media, Annu. Rev. Fluid Mech. **19**, 271 (1987).
[3] G. Rousseaux, A. De Wit, and M. Martin, Viscous fingering in packed chromatographic columns: Linear stability analysis, J. Chromatogr., A **1149**, 254 (2007).
[4] A. Riaz, M. Hesse, H. Tchelepi, and F. Orr, Onset of convection in a gravitationally unstable diffusive boundary layer in porous media, J. Fluid Mech. **548**, 87 (2006).
[5] P. Peñas-López, B. van Elburg, M. A. Parrales, and J. Rodríguez-Rodríguez, Diffusion of dissolved CO_2 in water propagating from a cylindrical bubble in a horizontal Hele-Shaw cell, Phys. Rev. Fluids **2**, 063602 (2017).
[6] A. D. Wit, Y. Bertho, and M. Martin, Viscous fingering of miscible slices, Phys. Fluids **17**, 054114 (2005).
[7] K. Ghesmat, H. Hassanzadeh, J. Abedi, and Z. Chen, Influence of nanoparticles on the dynamics of miscible Hele-Shaw flows, J. Appl. Phys. **109**, 104907 (2011).
[8] B. Dastvareh and J. Azaiez, Instabilities of nanofluid flow displacements in porous media, Phys. Fluids **29**, 044101 (2017).
[9] N. Sabet, H. Hassanzadeh, and J. Abedi, Control of viscous fingering by nanoparticles, Phys. Rev. E **96**, 063114 (2017).
[10] S. K. Das, S. U. Choi, W. Yu, and T. Pradeep, *Nanofluids: Science and Technology* (Wiley, New York, 2007).
[11] J. Foroozesh and S. Kumar, Nanoparticles behaviors in porous media: Application to enhanced oil recovery, J. Mol. Liq. **316**, 113876 (2020).
[12] M. C. Kim, C. K. Choi, and J.-K. Yeo, The onset of Soret-driven convection in a binary mixture heated from above, Phys. Fluids **19**, 084103 (2007).
[13] C. Tien and B. V. Ramarao, *Granular Filtration of Aerosols and Hydrosols* (Elsevier, New York, 2011).
[14] J. Buongiorno, Convective transport in nanofluids, J. Heat Transfer **128**, 240 (2006).
[15] B. Dastvareh and J. Azaiez, Thermophoretic effects on instabilities of nanoflows in porous media, J. Fluid Mech. **857**, 173 (2018).
[16] M. Zargartalebi and J. Azaiez, Mesoscopic study of miscible nanoflow instabilities, Phys. Fluids **30**, 024105 (2018).
[17] K. Ghesmat, H. Hassanzadeh, J. Abedi, and Z. Chen, Frontal stability of reactive nanoparticle transport during *in situ* catalytic upgrading of heavy oil, Fuel **107**, 525 (2013).
[18] N. Sabet, S. M. Jafari Raad, H. Hassanzadeh, and J. Abedi, Dynamics of miscible nanocatalytic reactive flows in porous media, Phys. Rev. Appl. **10**, 054033 (2018).
[19] B. Dastvareh and J. Azaiez, Instabilities of nonisothermal nanocatalytic reactive flows in porous media, Phys. Rev. Fluids **4**, 034003 (2019).
[20] B. Dastvareh, J. Azaiez, and P. A. Tsai, Nanocatalytic chemohydrodynamic instability: Deposition effects, Phys. Rev. E **100**, 053102 (2019).
[21] P. Jangir, R. Mohan, and P. Chokshi, Linear stability analysis of miscible displacement by nanofluid with concentration-dependent diffusivity, Chem. Eng. Sci. **240**, 116609 (2021).
[22] C. Tan and G. Homsy, Simulation of nonlinear viscous fingering in miscible displacement, Phys. Fluids **31**, 1330 (1988).
[23] W. Zimmerman and G. Homsy, Nonlinear viscous fingering in miscible displacement with anisotropic dispersion, Phys. Fluids **3**, 1859 (1991).
[24] P. Shukla and A. De Wit, Influence of the Péclet number on reactive viscous fingering, Phys. Rev. Fluids **5**, 014004 (2020).
[25] C. Rana, S. Pramanik, M. Martin, A. De Wit, and M. Mishra, Influence of Langmuir adsorption and viscous fingering on transport of finite size samples in porous media, Phys. Rev. Fluids **4**, 104001 (2019).
[26] W. Yu and H. Xie, A review on nanofluids: Preparation, stability mechanisms, and applications, J. Nanomater. **2012**, 435873 (2012).
[27] K. Ghesmat, H. Hassanzadeh, J. Abedi, and Z. Chen, Erratum: "Influence of nanoparticles on the dynamics of miscible Hele-Shaw flows" [J. Appl. Phys. **109**, 104907 (2011)], J. Appl. Phys. **121**, 189901 (2017).

[28] B. Dastvareh and J. Azaiez, Erratum: "Instabilities of nanofluid flow displacements in porous media" [Phys. Fluids **29**, 044101 (2017)], Phys. Fluids **29**, 079901 (2017).
[29] P. G. Saffman, Viscous fingering in Hele-Shaw cells, J. Fluid Mech. **173**, 73 (1986).
[30] M. Elimelech and C. R. O'Melia, Kinetics of deposition of colloidal particles in porous media, Environ. Sci. Technol. **24**, 1528 (1990).
[31] Y. Jin, M. V. Yates, S. S. Thompson, and W. A. Jury, Sorption of viruses during flow through saturated sand columns, Environ. Sci. Technol. **31**, 548 (1997).
[32] M. A. Marino, Distribution of contaminants in porous media flow, Water Resour. Res. **10**, 1013 (1974).
[33] F. Lindstrom and L. Boersma, Analytical solutions for convective-dispersive transport in confined aquifers with different initial and boundary conditions, Water Resour. Res. **25**, 241 (1989).
[34] M. T. Van Genuchten and W. J. Alves, *Analytical Solutions of the One-dimensional Convective-dispersive Solute Transport Equation*, Technical Bulletin Number 1661, U.S. Department of Agriculture, Agricultural Research Service (U.S. Department of Agriculture, Washington, DC, 1982).
[35] A. Mojtabi and M. O. Deville, One-dimensional linear advection–diffusion equation: Analytical and finite element solutions, Comput. Fluids **107**, 189 (2015).
[36] C. Tan and G. Homsy, Stability of miscible displacements in porous media: Rectilinear flow, Phys. Fluids **29**, 3549 (1986).
[37] T. K. Hota and M. Mishra, Non-modal stability analysis of miscible viscous fingering with non-monotonic viscosity profiles, J. Fluid Mech. **856**, 552 (2018).
[38] T. K. Hota, S. Pramanik, and M. Mishra, Nonmodal linear stability analysis of miscible viscous fingering in porous media, Phys. Rev. E **92**, 053007 (2015).
[39] W. M. Deen, *Analysis of Transport Phenomena* (Oxford University Press, New York, 1998).
[40] M. Bestehorn and A. Firoozabadi, Effect of fluctuations on the onset of density-driven convection in porous media, Phys. Fluids **24**, 114102 (2012).
[41] M. C. Kim, Linear and nonlinear analyses on the onset of gravitational instabilities in a fluid saturated within a vertical Hele-Shaw cell, Chem. Eng. Sci. **126**, 349 (2015).
[42] P. J. Schmid, Nonmodal stability theory, Annu. Rev. Fluid Mech. **39**, 129 (2007).
[43] COMSOL, COMSOL Multiphysics® V. 5.2, COMSOL AB, Stockholm Sweden.
[44] R. L. Van Dam, B. P. Eustice, D. W. Hyndman, W. W. Wood, and C. T. Simmons, Electrical imaging and fluid modeling of convective fingering in a shallow water-table aquifer, Water Resour. Res. **50**, 954 (2014).
[45] V. Sharma, S. Pramanik, and M. Mishra, Dynamics of a highly viscous circular blob in homogeneous porous media, Fluids **2**, 32 (2017).
[46] N. C. Mueller and B. Nowack, Nanoparticles for remediation: Solving big problems with little particles, Elements **6**, 395 (2010).